

# **INVESTIGATION OF FLUX PINNING PROPERTIES OF YBCO BASED NANOCOMPOSITES**

**GAURAV KUMAR**



**DEPARTMENT OF PHYSICS  
INDIAN INSTITUTE OF TECHNOLOGY DELHI  
JUNE 2025**

© Indian Institute of Technology Delhi (IITD), New Delhi, 2025

# **Investigation of Flux Pinning Properties of YBCO Based Nanocomposites**

*by*

**Gaurav Kumar**

Department of Physics

Submitted

In fulfillment of the requirements of the degree of Doctor of Philosophy  
to the



**INDIAN INSTITUTE OF TECHNOLOGY DELHI**

**JUNE 2025**

---

*Dedicated to my Family*

---

## Certificate

This is to certify that the thesis titled "**Investigation of Flux Pinning Properties of YBCO-Based Nanocomposites**," submitted by **Mr. Gaurav Kumar** to the **Indian Institute of Technology Delhi**, is a result of his original research work conducted under my guidance and supervision. The research presented in this thesis embodies the outcomes of a bona fide investigation carried out by Mr. Gaurav Kumar and meets the standards required for the degree of Doctor of Philosophy. The results presented herein have not been submitted, either in whole or in part, to any other university or institute for the award of any degree or diploma.



**Prof. Neeraj Khare**

Department of Physics

Indian Institute of Technology Delhi

Hauz Khas, New Delhi – 110016

India

## Acknowledgments

---

*For me, this thesis marks a significant milestone in my life, and I deeply cherish the journey that brought me here. I am profoundly grateful to the many individuals whose unwavering support, encouragement, and blessings have been instrumental in completing this endeavor. I take this opportunity to extend my heartfelt gratitude to everyone who has contributed, directly or indirectly, to the successful completion of this research and thesis.*

*I am deeply grateful to my supervisor, Prof. Neeraj Khare, for granting me the opportunity to pursue a PhD under his guidance and for his unwavering support throughout this journey. I greatly value his meticulous assistance in refining my academic writing, which has significantly enhanced my clarity and precision. His innovative thinking, enthusiasm, and positive attitude have been a constant source of inspiration, motivating me to conduct and complete my doctoral research with diligence and efficiency. I would also like to express my heartfelt gratitude to the Director of the Indian Institute of Technology Delhi and the DST-INSPIRE Fellowship, Department of Science and Technology (DST) for awarding me the INSPIRE Fellowship (IF190132). Their financial and institutional support has been pivotal in enabling me to successfully complete this thesis.*

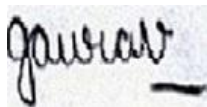
*I wish to express my sincere gratitude to Prof. Sujeet Chaudhary, Head of the Department of Physics, for his vital support and guidance throughout my PhD journey. I am equally thankful to my SRC members—Prof. Pankaj Srivastava, Prof. Sujeet Chaudhary, and Prof. Samaresh Das—for their valuable time, insightful evaluations of my work, and assistance in shaping this thesis to its best form. I would also like to extend my appreciation to the teams of the Nano-Research Scale Facility and the Central Research Facility of IIT Delhi, as well as the dedicated instrument*

*operators, whose efforts were instrumental in acquiring data in a timely manner. Their contributions have been crucial to the progress and completion of my research.*

*I would like to thank all of my seniors, Dr. Deepanshu Sharma, Dr. Sandeep Munjal, Dr. Surbhi Sharma, Dr. Sunil Kumar, Dr. Pratisha Gangwar, Dr. Huidrom Hemojit Singh, Dr. Mohd. Faraz, Dr. Dheeraj Kumar, Dr. Rohit Kumar, Dr. Mamta Dahiya, Dr. Amish Kumar Gautam, and Dr. Mohit Khosya for their moral support and guidance. I would also like to thank all my fellow lab mates: Mrs. Abhilasha Chouksey, Mr. Aman, Mr. Arun, Mr. Manoj, Mr. Sandeep, Ms. Rajni, and Ms. Sarita for their help in various ways and for providing a healthy atmosphere, which was essential for successfully completing my research work.*

*I'd like to acknowledge Dr. Rohit Kumar, Dr. Mamta Dahiya, and Dr. Tulja Bhavani Korukonda for providing experimental requisites, suggestions, and encouragement from time to time. A big shout out to Dr. Rohit Kumar, who has been a constant support, making my journey much smoother. I'd like to thank all my friends at IIT-D and beyond for making my time here such a joy. I am glad to have met Tulja, Balwant, Indraneel, Hardhyan, Mohan, Prabuddha Kant Mishra, Haribrahma Singh, Deepak, and Gaurav who have been my support system, making this place a home away from home.*

*Lastly, I would like to thank my family for their unconditional love, constant support, and encouragement, which have kept my spirits high as I pursued my ambitions.*



**Gaurav Kumar**

## ABSTRACT

---

YBa<sub>2</sub>Cu<sub>3</sub>O<sub>7- $\delta$</sub>  is a high-temperature superconductor that exhibits superconductivity above 77 K, surpassing the boiling point of liquid nitrogen. This material has garnered significant attention from the scientific community due to its exceptional characteristics, such as a high critical temperature ( $T_c$ ), a high upper critical field ( $H_{c2}$ ), and its ability to be synthesized in a single phase with ease. YBCO finds applications in various fields, such as transmission, power lines, magnetic resonance imaging, and levitation. However, its granular and porous structure can degrade its superconducting properties, resulting in lower critical current densities ( $J_c$ ). Achieving a high value of  $J_c$  under strong magnetic fields requires immobilizing vortices through flux pinning. Enhancing the critical current density ( $J_c$ ) and pinning force ( $F_p$ ) in YBCO is one of the main challenges, and several attempts have already been made. Therefore, the introduction of additional defects into the YBCO matrix, alongside natural ones, is essential to enhance its flux pinning properties. The best method to enhance flux pinning strength in YBCO is to add artificial pinning centers (APCs) in the form of nano additives. These nano additives, which can be made from metals, insulators, semiconductors, or magnetic materials and come in various morphologies such as nanoparticles, nanospheres, nanorods, or nanowires, are incorporated into the YBCO matrix, inducing defects that act as effective pinning centers to restrict vortex motion and improve pinning properties.

In order to carry out a study in this direction, YBCO-xKNbO<sub>3</sub> nanorods (NRs) or nanoparticles (NPs) ( $x = 0.0, 0.25, 0.5, \text{ and } 1.0 \text{ wt\%}$ ) nanocomposites are synthesized through a two-step process involving the hydrothermal method and solid-state reaction method, with their pinning properties being investigated. The orthorhombic phases of these samples are confirmed via X-ray

diffraction (XRD) patterns, and their morphology and composition are examined using field emission scanning electron microscopy (FESEM) and energy-dispersive X-ray spectroscopy (EDX). The superconducting critical temperature ( $T_{c0}$ ) of YBCO-xKNbO<sub>3</sub> ( $x = 0.25, 0.5, \text{ and } 1.0$  wt%) nanocomposite samples remains unchanged compared to the YBCO sample, indicating that small additions of KNbO<sub>3</sub> do not significantly affect  $T_{c0}$ . Magnetic measurements are conducted within a temperature range of 15 K to 65 K using a Magnetic Property Measurement System (MPMS). Adding 0.5 wt% NRs or NPs to the nanocomposite notably enhances the superconducting parameters, suggesting improved flux pinning properties. The sample with 0.5 wt% NPs exhibits a 4.4-fold increase in critical current density ( $J_c$ ), while the sample with 0.5 wt% NRs shows a 3.6-fold increase, indicating that KNbO<sub>3</sub>-NPs are more effective in improving the flux pinning and superconducting properties of YBCO. However, higher concentrations of NRs or NPs lead to reduced  $J_c$ , possibly due to increased agglomeration. The study also reveals that nanocomposites exhibit improved pinning properties, as the rate of  $J_c$  decrease is lower compared to pure YBCO under increasing external magnetic fields. Furthermore, magneto-transport measurements are conducted to calculate parameters such as activation energy ( $U_0$ ), coherence length ( $\xi(0)$ ), and upper critical field ( $H_{c2}(0)$ ). Samples containing 0.5 wt% KNbO<sub>3</sub>-NPs display increased derived parameters compared to YBCO and other nanocomposite samples, with the improvements being particularly pronounced in the YBCO-KNbO<sub>3</sub> NPs sample. This suggests that adding an appropriate quantity of KNbO<sub>3</sub>-NPs is a valuable strategy for advancing YBCO materials with significant practical application potential.

We investigate the effect of adding KNbO<sub>3</sub> nanoparticles to YBCO thin films. YBCO and YBCO-xKNbO<sub>3</sub> ( $x = 0.5$  and  $1.0$  wt%) nanocomposite thin films are deposited using the pulsed laser deposition technique on single-crystal SrTiO<sub>3</sub> (STO)(100) substrates. Structural,

morphological, transport, and magnetic properties are analyzed, with magnetic properties assessed using a Magnetic Property Measurement System (MPMS) in a magnetic field range of -7 T to +7 T. The YBCO-KNbO<sub>3</sub> nanocomposite thin films demonstrate enhanced performance compared to pure YBCO thin films. The most significant improvement—a 3.5-fold increase in critical current density ( $J_c$ ) and pinning properties—is observed in the YBCO-0.5wt%KNbO<sub>3</sub> thin film. Additionally, the nanocomposite thin films exhibit a slower rate of decay in  $J_c$  under increasing magnetic fields, indicating improved flux pinning properties. The lattice mismatch between YBCO and KNbO<sub>3</sub>-NPs appears to introduce additional defects, contributing to the enhancement of flux pinning. These results suggest that incorporating small amounts of KNbO<sub>3</sub>-NPs effectively enhances the in-field performance of YBCO thin films.

## सारांश

---

$\text{YBa}_2\text{Cu}_3\text{O}_{7-\delta}$  एक उच्च तापमान सुपरकंडक्टर है, जो 77 K से ऊपर के तापमान पर सुपरकंडक्टिविटी प्रदर्शित करता है, जो कि तरल नाइट्रोजन के उबाल बिंदु से अधिक है। इसके असाधारण गुणों, जैसे उच्च क्रिटिकल तापमान ( $T_c$ ), उच्च ऊपरी क्रिटिकल क्षेत्र ( $H_{c2}$ ), और इसे एकल चरण में आसानी से संश्लेषित करने की क्षमता के कारण, इस सामग्री ने वैज्ञानिक समुदाय का विशेष ध्यान आकर्षित किया है। YBCO का उपयोग विभिन्न क्षेत्रों में किया जाता है, जैसे विद्युत संचार, पावर लाइन्स, मैग्नेटिक रेजोनेंस इमेजिंग, और लेविटेशन। हालांकि, इसका दानेदार और छिद्रयुक्त संरचना इसकी सुपरकंडक्टिंग विशेषताओं को कमजोर कर सकती है, जिससे क्रिटिकल करंट घनत्व ( $J_c$ ) कम हो जाता है। मजबूत चुंबकीय क्षेत्रों के तहत  $J_c$  के उच्च मान को प्राप्त करने के लिए, फ्लक्स पिनिंग के माध्यम से वर्टिसेस को स्थिर करना आवश्यक है। YBCO में क्रिटिकल करंट घनत्व ( $J_c$ ) और पिनिंग फोर्स ( $F_p$ ) को बढ़ाना एक प्रमुख चुनौती है, और इसके लिए कई प्रयास किए गए हैं। इसलिए, YBCO मैट्रिक्स में प्राकृतिक दोषों के साथ-साथ अतिरिक्त दोषों का परिचय आवश्यक है ताकि इसकी फ्लक्स पिनिंग विशेषताओं में सुधार हो। YBCO में फ्लक्स पिनिंग की ताकत बढ़ाने का सबसे अच्छा तरीका नैनो एडिटिक्स के रूप में कृत्रिम पिनिंग सेंटर (APCs) को जोड़ना है। ये नैनो एडिटिक्स धातु, इन्सुलेटर, सेमीकंडक्टर या चुंबकीय सामग्रियों से बने हो सकते हैं और विभिन्न रूपों में आते हैं, जैसे नैनोपार्टिकल्स, नैनोस्पीयर्स, नैनोरोड्स, या नैनोवायर। इन्हें YBCO मैट्रिक्स में सम्मिलित किया जाता है, जिससे ऐसे दोष उत्पन्न होते हैं जो प्रभावी पिनिंग सेंटर के रूप में कार्य करते हैं, वर्टेक्स की गति को रोकते हैं और पिनिंग गुणों में सुधार करते हैं।

इस दिशा में अध्ययन करने के लिए,  $\text{YBCO-xKNbO}_3$  नैनोरोड्स (NRs) या नैनोपार्टिकल्स (NPs) ( $x = 0.0, 0.25, 0.5, \text{ and } 1.0 \text{ wt\%}$ ) नैनोकंपोजिट नमूनों को हाइड्रोथर्मल और सॉलिड-स्टेट रिएक्शन विधियों के

माध्यम से दो-चरणीय प्रक्रिया के तहत संश्लेषित किया गया, और उनकी फ्लक्स पिनिंग विशेषताओं की जांच की गई। इन नमूनों के ऑर्थोरोम्बिक चरणों की पुष्टि एक्स-रे विवर्तन (XRD) पैटर्न द्वारा की गई, और उनकी संरचना और संरचना की जांच फील्ड एमिशन स्कैनिंग इलेक्ट्रॉन माइक्रोस्कोपी (FESEM) और ऊर्जा-डिस्पर्सिव एक्स-रे स्पेक्ट्रोस्कोपी (EDX) द्वारा की गई।  $\text{YBCO-xKNbO}_3$  ( $x = 0.25, 0.5, \text{ and } 1.0$  wt%) नैनोकंपोजिट नमूनों के सुपरकंडक्टिंग क्रिटिकल तापमान ( $T_{c0}$ ) में YBCO नमूने की तुलना में कोई परिवर्तन नहीं देखा गया, जो यह दर्शाता है कि  $\text{KNbO}_3$  की छोटी मात्रा जोड़ने से  $T_{c0}$  पर कोई महत्वपूर्ण प्रभाव नहीं पड़ता। चुंबकीय मापन 15 K से 65 K के तापमान सीमा में मैग्नेटिक प्रॉपर्टी मेजरमेंट सिस्टम (MPMS) का उपयोग करके किया गया। नैनोकंपोजिट में 0.5 wt% NRs या NPs जोड़ने से सुपरकंडक्टिंग मापदंडों में उल्लेखनीय सुधार हुआ, जो फ्लक्स पिनिंग गुणों में सुधार का संकेत देता है। 0.5 wt% NPs वाले नमूने में क्रिटिकल करंट घनत्व ( $J_c$ ) में 4.4 गुना वृद्धि देखी गई, जबकि 0.5 wt% NRs वाले नमूने में 3.6 गुना वृद्धि हुई, जो यह दर्शाता है कि  $\text{KNbO}_3$ -NPs YBCO के फ्लक्स पिनिंग और सुपरकंडक्टिंग गुणों को बेहतर बनाने में अधिक प्रभावी हैं। हालांकि, NRs या NPs की उच्च सांद्रता से  $J_c$  में कमी आई, जो संभवतः बड़े हुए एग्लोमरेशन के कारण हुई। अध्ययन से यह भी पता चला कि नैनोकंपोजिट में पिनिंग गुणों में सुधार हुआ, क्योंकि बाहरी चुंबकीय क्षेत्रों के बढ़ने पर  $J_c$  की गिरावट की दर शुद्ध YBCO की तुलना में कम थी। इसके अलावा, मैग्नेटो-ट्रांसपोर्ट मापन का उपयोग करके सक्रियण ऊर्जा ( $U_0$ ), कोहेरेन्स लंबाई ( $\xi(0)$ ), और ऊपरी क्रिटिकल क्षेत्र ( $H_{c2}(0)$ ) जैसे मापदंडों की गणना की गई। 0.5 wt%  $\text{KNbO}_3$ -NPs वाले नमूनों ने YBCO और अन्य नैनोकंपोजिट नमूनों की तुलना में बेहतर प्राप्त मापदंड दिखाए, विशेष रूप से YBCO- $\text{KNbO}_3$  NPs नमूने में। यह सुझाव देता है कि  $\text{KNbO}_3$ -NPs की उपयुक्त मात्रा जोड़ने से YBCO सामग्री में महत्वपूर्ण व्यावहारिक अनुप्रयोग क्षमता के साथ सुधार किया जा सकता है।

हमने YBCO पतली परतों में  $\text{KNbO}_3\text{-NPs}$  जोड़ने के प्रभावों का अध्ययन किया। YBCO और YBCO- $x\text{KNbO}_3$  ( $x = 0.5$  और  $1.0$  wt%) नैनोकंपोजिट पतली परतों को पल्स लेजर डिपोजिशन तकनीक का उपयोग करके सिंगल क्रिस्टल  $\text{SrTiO}_3$  (STO)(100) सबस्ट्रेट्स पर जमा किया गया। संरचनात्मक, भौतिक, परिवहन, और चुंबकीय गुणों का विश्लेषण किया गया, जिसमें चुंबकीय गुणों का आकलन  $-7$  T से  $+7$  T के चुंबकीय क्षेत्र सीमा में MPMS का उपयोग करके किया गया। YBCO- $\text{KNbO}_3$  नैनोकंपोजिट पतली परतों ने शुद्ध YBCO पतली परतों की तुलना में बेहतर प्रदर्शन दिखाया। सबसे उल्लेखनीय सुधार, क्रिटिकल करंट घनत्व ( $J_c$ ) और पिनिंग गुणों में  $3.5$  गुना वृद्धि, YBCO- $0.5\text{wt}\%\text{KNbO}_3$  पतली परत में देखी गई। इसके अलावा, नैनोकंपोजिट पतली परतों ने बढ़ते चुंबकीय क्षेत्रों के तहत  $J_c$  के क्षय की धीमी दर दिखाई, जो बेहतर पिनिंग गुणों को इंगित करता है। YBCO और  $\text{KNbO}_3\text{-NPs}$  के बीच लेटिस मिसमैच अतिरिक्त दोषों को पेश करता प्रतीत होता है, जिससे फ्लक्स पिनिंग गुणों में सुधार होता है। इन परिणामों से पता चलता है कि  $\text{KNbO}_3\text{-NPs}$  की छोटी मात्रा को शामिल करने से YBCO की इन-फील्ड प्रदर्शन क्षमता प्रभावी रूप से बढ़ सकती है।

## Table of Contents

---

<b>Certificate</b>	<b>i</b>
<b>Acknowledgment</b>	<b>ii</b>
<b>Abstract</b>	<b>iv</b>
<b>Table of Contents</b>	<b>x</b>
<b>List of Figures</b>	<b>xv</b>
<b>List of Tables</b>	<b>xxi</b>
<b>Chapter 1: Introduction</b>	<b>1-36</b>
1.1 History of Superconductivity	2
1.2 The Phenomena of Superconductivity	4
1.2.1 Electrical Resistance	4
1.2.2 Meissner Effect	5
1.2.3 The Penetration Depth, $\lambda$	6
1.2.4 The Coherence Length, $\xi$	7
1.3 Types of Superconductors	8
1.3.1 Type-I Superconductor	8
1.3.2 Type-II Superconductor	9
1.4 High-Temperature Superconductors (HTS)	10
1.5 YBa <sub>2</sub> Cu <sub>3</sub> O <sub>7-<math>\delta</math></sub> : A High-Temperature Superconductor (HTS)	11
1.5.1 Crystal Structure	11
1.5.2 Physical Parameter	13
1.5.3 Bulk YBCO	14
1.5.4 YBCO Thin Film	15
1.5.5 Flux Pinning	17
1.5.5.1 Natural Pinning Centers	19
1.5.5.2 Artificial Pinning Centers	22
1.6 Motivation of the Work	26
1.7 Objective of the Present Thesis	27
1.8 Organization of the Thesis	27

References	34
<b>Chapter 2: Experimental Techniques &amp; Sample Characterizations</b>	<b>37-70</b>
2.1 Introduction	38
2.2 Sample Preparation	38
2.2.1 Hydrothermal Method	39
2.2.2 Solid State Reaction Method	41
2.3 Preparation of Superconducting Thin Films	42
2.3.1 Thin Film Deposition Techniques	42
2.3.1.1 Pulsed Laser Deposition Technique	43
2.4 Characterization Techniques	46
2.4.1 Structural and Surface Morphological Characterization	47
2.4.1.1 X-Ray Diffraction	47
2.4.1.2 Energy Dispersive X-Ray Spectroscopy (EDS)	50
2.4.1.3 Scanning Electron Microscopy (SEM)	52
2.4.1.4 Transmission Electron Microscopy (TEM)	54
2.4.2 Resistivity Measurements	56
2.4.2.1 DC Resistivity Measurement Using the Four-Probe Method	56
2.4.3 Magnetic Measurements	58
2.4.3.1 Physical Property Measurement System (PPMS)	58
2.4.3.1.1 Vibrating Sample Magnetometer (VSM)	58
2.4.3.1.2 DC and AC Electrical Resistivity Measurements	61
2.4.3.2 Magnetic Property Measurement System (MPMS)	64
2.4.3.3 Critical Current Density ( $J_c$ ) and Pinning Force Density ( $F_p$ )	66
References	68
<b>Chapter 3: Study of Critical Current and Flux Pinning in YBCO- KNbO<sub>3</sub> (Nanorods) Nanocomposite Superconductor</b>	<b>71-93</b>
3.1 Introduction	72
3.2 Experimental Details	75
3.2.1 Synthesis Processes	75

3.2.1.1 Synthesis of KNbO <sub>3</sub> Nanorods, YBCO, and YBCO-xKNbO <sub>3</sub> Nanocomposites	75
3.2.2 Characterization Technique	76
3.3 Results and Discussion	76
3.3.1 Structural Investigation	76
3.3.1.1 X-Ray Diffraction Study	76
3.3.2 Microstructural Study	78
3.3.2.1 Scanning Electron Microscopy Study	78
3.3.3 Electrical Resistivity Measurements	80
3.3.3.1 Electrical Transport Measurement of YBCO and YBCO-xKNbO <sub>3</sub> Nanocomposites	80
3.3.4 Magnetic Measurements	82
3.3.4.1 Analysis of Magnetic Hysteresis Loops	82
3.3.4.2 Critical Current Density ( $J_c$ ) and Pinning Force Density ( $F_p$ )	83
3.4 Conclusions	89
References	91

## **Chapter 4: Study of Critical Current and Flux Pinning in YBCO-KNbO<sub>3</sub> (Nanoparticles) Nanocomposite Superconductor** **94-112**

4.1 Introduction	95
4.2 Experimental Details	96
4.2.1 Synthesis Procedure	96
4.2.1.1 Synthesis of KNbO <sub>3</sub> Nanoparticles, YBCO, and YBCO-xKNbO <sub>3</sub> Nanocomposites	96
4.2.2 Techniques for Characterization	96
4.3 Results and Discussion	97
4.3.1 Studies on Structures	97
4.3.1.1 X-Ray Diffraction Study	97
4.3.2 Microstructural Study	98
4.3.2.1 Scanning Electron Microscopy and Transmission Electron Microscopy Study	98
4.3.3 Electrical Measurements	101

4.3.3.1 Electrical Transport Measurement of YBCO and YBCO-xKNbO <sub>3</sub> Nanocomposites	101
4.3.4 Magnetic Measurements	102
4.3.4.1 Analysis of Magnetic Hysteresis Loops	102
4.3.4.2 Critical Current Density ( $J_c$ ) and Pinning Force Density ( $F_p$ )	103
4.4 Conclusions	109
References	110

**Chapter 5: Magneto-resistivity Study of YBCO-KNbO<sub>3</sub> (Nanorods or Nanoparticles) Nanocomposite Superconductor 113-132**

5.1 Introduction	114
5.2 Experimental Details	116
5.2.1 Synthesis Methodology	116
5.2.2 Characterization Techniques	116
5.3 Results and Discussions	116
5.3.1 Structural Analysis	116
5.3.1.1 X-Ray Diffraction Study	116
5.3.2 Study of the morphology of YBCO and its nanocomposite	117
5.3.2.1 Transmission Electron Microscopy and Scanning Electron Microscopy Study	117
5.3.3 Analysis of Magneto-Resistivity	119
5.3.3.1 Electrical Transport Measurement of YBCO and YBCO-xKNbO <sub>3</sub> Nanocomposites	119
5.3.4 Field-dependent variations in the activation energy $U_0$	123
5.3.5 The upper critical field $H_{c2}(0)$ and the coherence length $\xi(0)$	127
5.4 Conclusions	130
References	131

**Chapter 6: Study of Critical Current and Flux Pinning in YBCO-KNbO<sub>3</sub> (Nanoparticles) Nanocomposite Thin Films 133-148**

6.1 Introduction	134
6.2 Experimental Details	135
6.2.1 Film Deposition	135

6.2.1.1 Deposition of YBCO and YBCO-xKNbO <sub>3</sub> Nanocomposite thin films	135
6.2.2 Characterization Technique	136
6.3 Results and Discussion	136
6.3.1 Structural Investigation	136
6.3.1.1 X-Ray Diffraction Study	136
6.3.2 Electrical Resistivity Measurements	137
6.3.2.1 Electrical Transport Measurement of YBCO-xKNbO <sub>3</sub> (x = 0.0, 0.5, and 1.0 wt%) Nanocomposite thin films	137
6.3.3 Magnetic Measurements	139
6.3.3.1 Analysis of Magnetic Hysteresis Loops	139
6.3.3.2 Critical Current Density (J <sub>c</sub> ) and Pinning Force Density (F <sub>p</sub> )	140
6.4 Conclusions	144
References	146
<b>Chapter 7: Conclusions and Future Scope</b>	<b>149-153</b>
7.1 Summary	150
7.2 Future Perspective	153
<b>Publications in International Journals</b>	154
<b>Poster/Oral presentation at National/International Conferences</b>	155
<b>Author's Biography</b>	156

## List of Figures

---

- Figure 1.1** Examining the contrasting temperature-dependent electrical resistivity behavior between superconducting materials, characterized by zero resistivity, and normal materials.
- Figure 1.2** A typical critical surface for a superconductor illustrates the interdependence of critical parameters.
- Figure 1.3** The resistance variation of mercury (Hg) plotted against temperature.
- Figure 1.4** Magnetic field response to superconductor: (a) Penetration of magnetic flux for  $T > T_c$ , (b) Expulsion of magnetic flux from the interior of superconductor for  $T < T_c$ .
- Figure 1.5** The penetration of the magnetic field near the surface of a superconductor reveals that the magnetic field  $B_0$  diminishes from the surface to  $B_0/e$  at a distance  $x = \lambda$  from the surface.
- Figure 1.6** The change in magnetization concerning the applied field is depicted for (a) Type-I and (b) Type-II superconductors.
- Figure 1.7** Schematic illustration: (a) depicts the orthorhombic structure of pristine YBCO with  $\delta = 0.4$ , while (b) showcases the tetragonal structure of pristine YBCO with  $\delta = 1$ .
- Figure 1.8** Changes in the magnetic field as a function of temperature for (a) Type-I and (b) Type-II superconductors.
- Figure 1.9** Mixed state in Type-II superconductor.
- Figure 1.10** Schematic representations of different naturally arising defects encountered during the thin film growth process, serving as flux pinning sites.

- Figure 2.1** The hydrothermal setup used for nanostructure synthesis includes (a) a Teflon cup, (b) a stainless-steel autoclave, and (c) a hot air oven.
- Figure 2.2** The solid-state reaction method for calcination and sintering involves the use of (a) a mortar and pestle, (b) a tubular furnace, and (c) an alumina crucible.
- Figure 2.3** Schematic of PLD technique.
- Figure 2.4** X-ray diffraction from a series of atomic planes in accordance with Bragg's condition.
- Figure 2.5** (a) Diagram illustrating the setup of an X-ray diffractometer. (b) Bruker D8 Advance powder X-ray diffractometer model.
- Figure 2.6** Schematic diagram showing the working principle of EDS.
- Figure 2.7** (a) Diagram showing the electron beam in SEM, (b) Volume of interaction between the electron beam and the sample.
- Figure 2.8** The experimental set-up of SEM (Zeiss EVO 50).
- Figure 2.9** Experimental setup of the TEM instrument.
- Figure 2.10** (a) Diagram illustrating the four-probe configuration for resistivity measurement, (b) A photograph of a cryocooler, and (c) Schematic illustrating the components utilized in measuring the temperature dependency of resistivity with a Cryocooler.
- Figure 2.11** The PPMS apparatus (left), a probe situated within the Dewar (center), and the sample area inside the magnet, encompassing the VSM coil and sample puck for transport measurements (right).
- Figure 2.12** Schematic diagram for the operation of PPMS instrument (for CFMS-PPMS Cryogenics Ltd).
- Figure 2.13** Diagram for the internal instrumentation of PPMS (for CFMS-PPMS Cryogenics

Ltd).

**Figure 2.14** Schematic diagram for the Resistivity Probe in the PPMS CFMS-PPMS Cryogenics Ltd.

**Figure 2.15** Whole setup for the measurement of resistivity in the temperature range of 10 - 110 K under the magnetic field of 0 - 7 T.

**Figure 2.16** Experimental configuration used for magnetic evaluations of the sample.

**Figure 3.1** XRD pattern of YBCO, KNbO<sub>3</sub>-NRs, and YBCO-xKNbO<sub>3</sub> nanocomposite samples (x = 0.25, 0.5, and 1.0 wt%), respectively.

**Figure 3.2** FESEM image and EDX spectra, as well as the elemental composition in (a, b) KNbO<sub>3</sub>-NRs, (c, d) YBCO, (e, f) YBCO-0.5wt%KNbO<sub>3</sub>, and (g, h) YBCO-1.0wt%KNbO<sub>3</sub> nanocomposite sample, respectively.

**Figure 3.3**  $\rho$  vs. temperature for YBCO-xKNbO<sub>3</sub> nanocomposite samples (x = 0.0, 0.25, 0.5, and 1.0 wt%), respectively.

**Figure 3.4** Variation of (a)  $\rho_0$  and (b)  $\alpha$  vs. wt% concentration of KNbO<sub>3</sub>-NRs content in YBCO and YBCO-xKNbO<sub>3</sub> nanocomposites (x = 0.25, 0.5, and 1.0 wt%), respectively.

**Figure 3.5** Variation of  $T_{c0}$  vs. wt% concentration of KNbO<sub>3</sub>-NRs.

**Figure 3.6** M(H) loops for 0.0, 0.25, 0.5, and 1.0 wt% concentration of KNbO<sub>3</sub>-NRs added YBCO at temperatures of (a) 15 K and (b) 65 K, respectively.

**Figure 3.7**  $J_c$  vs. the external magnetic field for YBCO and YBCO-xKNbO<sub>3</sub> nanocomposite samples (x = 0.25, 0.5, and 1.0 wt%) at (a) 15 K, (b) 65 K, and (c) variation of  $J_{cmax}$  with wt% of KNbO<sub>3</sub>-NRs concentration in YBCO-KNbO<sub>3</sub> nanocomposite samples at 15 K and 65 K, respectively.

**Figure 3.8**  $\alpha$  vs. temperature for YBCO and YBCO-xKNbO<sub>3</sub> nanocomposite samples (x = 0.25, 0.5, and 1.0 wt%), where the inset image shows the change of  $J_c$  with the applied

field on a double logarithmic scale for pure YBCO at 15 K.

- Figure 3.9** Variation of  $F_p$  for 0.0, 0.25, 0.5, and 1.0 wt%  $\text{KNbO}_3$ -NRs added YBCO sample with the applied magnetic field at (a) 15 K, (b) 65 K, (c) variation of  $F_{p\max}$  with wt% of  $\text{KNbO}_3$ -NRs concentration in YBCO- $\text{KNbO}_3$  nanocomposite samples at 15 K and 65 K, and (d)  $F_{p\max}$  temperature variation for YBCO and YBCO- $x\text{KNbO}_3$  nanocomposite samples ( $x = 0.25, 0.5, \text{ and } 1.0 \text{ wt}\%$ ), respectively.
- Figure 4.1** XRD patterns of the YBCO compound,  $\text{KNbO}_3$ -NPs, and YBCO- $x\text{KNbO}_3$  nanocomposites for  $x = 0.25, 0.5, \text{ and } 1.0 \text{ wt}\%$ , respectively.
- Figure 4.2** (a) Scanning Electron Microscopic (SEM) image, (b) Transmission Electron Microscopic (TEM) image, and (c) Energy Dispersive X-Ray (EDX) spectra of  $\text{KNbO}_3$  nanoparticles.
- Figure 4.3** Scanning Electron Microscopic (SEM) images of (a) YBCO compound, (c) YBCO-0.25wt% $\text{KNbO}_3$ , (e) YBCO-1.0wt% $\text{KNbO}_3$  nanocomposite, and Energy Dispersive X-Ray (EDX) spectra of (b) YBCO compound, (d) YBCO-0.25wt% $\text{KNbO}_3$ , (f) YBCO-1.0wt% $\text{KNbO}_3$  nanocomposite, respectively.
- Figure 4.4** (a) Normalized resistivity as a function of temperature for YBCO- $x\text{KNbO}_3$  nanocomposites ( $x = 0.0, 0.25, 0.5, \text{ and } 1.0 \text{ wt}\%$ ) (b) critical temperature vs. concentration of  $\text{KNbO}_3$  in YBCO- $x\text{KNbO}_3$  nanocomposites for  $x = 0.0, 0.25, 0.5, \text{ and } 1.0 \text{ wt}\%$ , respectively.
- Figure 4.5** DC magnetization measurement for YBCO- $x\text{KNbO}_3$  ( $x = 0.0, 0.25, 0.5, \text{ and } 1.0 \text{ wt}\%$ ) using externally applied field up to 6 T at (a) 15 K, (b) 65 K, respectively.
- Figure 4.6** Critical current density ( $J_c$ ) vs. applied field curve for YBCO- $x\text{KNbO}_3$  ( $x = 0.0, 0.25, 0.5, \text{ and } 1.0 \text{ wt}\%$ ) nanocomposites at (a) 15 K, (b) 65 K, and (c) variation of  $J_{c\max}$  with NPs concentration in the nanocomposites at 15 and 65 K, respectively.
- Figure 4.7** Exponent ( $\alpha$ ) vs. temperature curve for nanocomposite YBCO- $x\text{KNbO}_3$  ( $x = 0.0, 0.25, 0.5, \text{ and } 1.0 \text{ wt}\%$ ). The inset Figure displays the slope of the linear fitted

curve on  $J_c$  double log scale with an applied field for YBCO at 15 K.

**Figure 4.8** Pinning force density ( $F_p$ ) vs. applied field curve for YBCO-xKNbO<sub>3</sub> nanocomposites ( $x = 0.0, 0.25, 0.5,$  and  $1.0$  wt%) at (a) 15 K, (b) 65 K, (c) variation of  $F_{pmax}$  with wt% of KNbO<sub>3</sub> concentration in YBCO-KNbO<sub>3</sub> nanocomposite samples at 15 K and 65 K, and (d) temperature-dependent variation in  $F_{pmax}$  value in nanocomposites, respectively.

**Figure 5.1** X-ray diffraction (XRD) patterns of (a) KNbO<sub>3</sub>-NRs and KNbO<sub>3</sub>-NPs, and (b) YBCO, YBCO-KNbO<sub>3</sub> NRs, and YBCO-KNbO<sub>3</sub> NPs nanocomposite sample.

**Figure 5.2** TEM image of (a) KNbO<sub>3</sub>-NPs and (b) KNbO<sub>3</sub>-NRs, SEM image of (c) YBCO, (e) YBCO-KNbO<sub>3</sub> NRs, (g) YBCO-KNbO<sub>3</sub> NPs nanocomposite samples, and EDS spectra of (d) YBCO, (f) YBCO-KNbO<sub>3</sub> NRs, (h) YBCO-KNbO<sub>3</sub> NPs nanocomposite samples.

**Figure 5.3** Variations in the temperature-dependent normalized resistivity ( $\rho/\rho_{110}$ ) across a range of applied magnetic fields, ranging from 0.1 to 7 T for (a) YBCO sample, (b) YBCO-KNbO<sub>3</sub> NRs, and (c) YBCO-KNbO<sub>3</sub> NPs added nanocomposite samples.

**Figure 5.4** Arrhenius graph showing a change in  $\ln(\rho/\rho_{110})$  against  $1/T$  across various applied magnetic fields ranging from 0.1 to 7 T for (a) pure YBCO, (b) YBCO-KNbO<sub>3</sub> NRs, and (c) YBCO-KNbO<sub>3</sub> NPs added nanocomposite samples.

**Figure 5.5** Variations in the activation energy ( $U_0$ ) with applied magnetic field for (a) YBCO sample, (b) YBCO-KNbO<sub>3</sub> NRs, and (c) YBCO-KNbO<sub>3</sub> NPs added nanocomposite samples.

**Figure 5.6** Variations in the activation energy ( $U_0$ ) with an external applied magnetic field, derived from conventional TAFF theories and fitted using a power law,  $U_0(H) \sim H^{(-\alpha)}$  for (a) YBCO sample, (b) YBCO-KNbO<sub>3</sub> NRs, and (c) YBCO-KNbO<sub>3</sub> NPs added nanocomposite samples.

- Figure 5.7** The temperature-dependent behavior of the upper critical field,  $H_{c2}(T)$  (at 50% of  $\rho_n$ ), was analyzed by fitting it with the Ginzburg-Landau theory for (a) YBCO, (b) YBCO-KNbO<sub>3</sub> NRs, and (c) YBCO-KNbO<sub>3</sub> NPs added nanocomposite samples.
- Figure 6.1** XRD pattern for YBCO, KNbO<sub>3</sub>-NPs, and YBCO-xKNbO<sub>3</sub> (x = 0.5 and 1.0 wt%) nanocomposite films, respectively.
- Figure 6.2** Resistance vs. Temperature curve for YBCO-xKNbO<sub>3</sub> (x = 0.0, 0.5, and 1.0 wt%) nanocomposite films.
- Figure 6.3** M(H) loops for YBCO-xKNbO<sub>3</sub> (x = 0.0, 0.5, and 1.0 wt%) nanocomposite films at temperatures of (a) 15 K and (b) 65 K, respectively.
- Figure 6.4** Variation of  $J_c$  with the external magnetic field for YBCO-xKNbO<sub>3</sub> (x = 0.0, 0.5, and 1.0 wt%) nanocomposite films at (a) 15 K and (b) 65 K. (c) Variation of  $J_{cmax}$  with the wt% of KNbO<sub>3</sub> nanoparticles concentration in YBCO-KNbO<sub>3</sub> nanocomposite thin films at temperatures of 15 K and 65 K.
- Figure 6.5** Variation of improvement factor “ $f$ ” with externally applied field ranging from 0 to 7 T at 65 K.
- Figure 6.6** The study examines the change in pinning force ( $F_p$ ) for YBCO thin films with the addition of 0.0 to 1.0 wt% KNbO<sub>3</sub>-NPs under externally applied magnetic fields at temperatures (a) 15 K and (b) 65 K.

## List of Tables

---

- Table 1.1** The values of various superconducting parameters such as critical temperature ( $T_c$ ), lower critical magnetic field ( $H_{c1}$ ), and upper critical magnetic field ( $H_{c2}$ ) values for certain Type-II superconductors.
- Table 1.2** Various physical parameters for YBCO superconductor.
- Table 1.3** Diverse single crystal substrates employed in depositing thin films of YBCO.
- Table 1.4** Various perovskite and other oxide materials are used as additives in YBCO compounds.
- Table 2.1** Operating parameters for Nd:YAG LASER used.
- Table 5.1** The critical transition temperature values ( $T_c^{\text{onset}}$  and  $T_{c0}$ ) and the width of transition ( $\Delta T$ ) for pure YBCO, YBCO-KNbO<sub>3</sub> NRs, and YBCO-KNbO<sub>3</sub> NPs under different magnetic fields.
- Table 5.2** Parameters for the upper critical magnetic field and coherence length are determined using the Ginzburg-Landau model for YBCO, as well as for nanocomposites incorporating YBCO-KNbO<sub>3</sub> NRs and YBCO-KNbO<sub>3</sub> NPs.